Geophysical Research Letters

RESEARCH LETTER
10.1029/2023GL105083

Tropical Convection Overshoots the Cold Point Tropopause Nearly as Often Over Warm Oceans as Over Land

Jacqueline M. Nugent[1] and **Christopher S. Bretherton**[1,2]

[1]Department of Atmospheric Sciences, University of Washington, Seattle, WA, USA, [2]Allen Institute for Artificial Intelligence, Seattle, WA, USA

Key Points:

- We identify likely tropical cold point overshoots using a radar/lidar calibrated cold point-relative brightness temperature proxy
- In a 4-year climatology, cold point overshoots only modestly favor convectively active land areas over the Indo-Pacific warm pool
- Thin cirrus above the cold point covers over 100-fold more tropical area than cold point overshoots

Supporting Information:

Supporting Information may be found in the online version of this article.

Correspondence to:

J. M. Nugent,
jnug@uw.edu

Citation:

Nugent, J. M., & Bretherton, C. S. (2023). Tropical convection overshoots the cold point tropopause nearly as often over warm oceans as over land. *Geophysical Research Letters*, *50*, e2023GL105083. https://doi.org/10.1029/2023GL105083

Received 23 JUN 2023
Accepted 3 OCT 2023

Abstract Tropical convection that overshoots the cold point tropopause can impact the climate by directly influencing water vapor, temperatures, and thin cirrus in the upper troposphere-lower stratosphere (UTLS) region. The distribution of cold point overshoots between land and ocean may help determine how the overshoots will affect the UTLS in a changing climate. Using 4 years of satellite and reanalysis data, we test a brightness temperature proxy calibrated by radar/lidar data to identify cold point-overshooting convection across the global tropics. We find evidence of cold point-overshooting convection throughout the tropics, though other cirrus above the cold point cover an area 100 times larger than overshooting tops. Cold point-overshooting convection occurs 30%–40% more often over convectively active land areas than over the warmest oceans. This proxy can be generalized to evaluate the fidelity of cold point overshoots simulated by storm-resolving models.

Plain Language Summary Extremely deep convection in the tropics that overshoots the cold point, the coldest temperature level between the upper troposphere and lower stratosphere, influences the vertical temperature structure of this region and water vapor in the lower stratosphere, where it acts as a greenhouse gas. Overshooting cloud tops appear "cold" in infrared satellite imagery, so they can be identified from the difference between their brightness temperature and the nearby cold point temperature. We calibrate this brightness temperature proxy using satellite measurements of cloud ice. Cold point overshoots occur almost as often over the warmest oceans as over moist tropical land areas. Overshooting tops comprise only 1% of satellite-detectable cloud above the cold point, most of which is very thin ice cloud. Our proxy can be used as a real-world observational test of cold point overshoots simulated by the most realistic global atmospheric models, which resolve individual thunderstorm systems.

1. Introduction

The tropical upper troposphere-lower stratosphere region (UTLS, ~12–20 km) plays a critical role in the Earth's climate by influencing the composition of the lower stratosphere. The Brewer-Dobson circulation helps loft air from the upper troposphere into the lower stratosphere, which gets "freeze-dried" as it passes through the coldest temperatures near the tropopause, helping to set stratospheric moisture content (Brewer, 1949; Dessler, 2002; Holton & Gettelman, 2001). This mechanism is robust in observations; variations in stratospheric moisture are highly correlated with variations in the cold point temperature on subseasonal to interannual time scales (e.g., Randel & Jensen, 2013; Randel et al., 2004; Zhou et al., 2001). This is significant for climate change. Many climate models project stratospheric water vapor will increase under 21st century greenhouse warming (Dessler et al., 2016; Tian et al., 2023), producing an additional greenhouse effect which would further increase the surface warming rate (Solomon et al., 2010).

However, this is a challenging modeling problem. In addition to nonlocal dynamical drivers, a complex, multiscale mixture of local physical processes is thought to regulate the cold point and overlying lower stratosphere. Though infrequent, convection that overshoots the cold point can alter the cold point temperature through entrainment (Chae et al., 2011; Gettelman et al., 2002; Kuang & Bretherton, 2004; Randel & Park, 2019) and modify stratospheric air through turbulent mixing of ice and water vapor (e.g., Corti et al., 2008; Dion et al., 2019; Ueyama et al., 2023) and removal of vapor by deposition onto sedimenting ice crystals (Jensen et al., 2007; Khaykin et al., 2022). Observations during the southeast Asian monsoon suggest ice injected by convective overshoots over land strongly affects the regional UTLS composition (Bucci et al., 2020). Cold point-overshooting convection may drive much of the transport between the upper troposphere and lower stratosphere (Pommereau, 2010;

Vernier et al., 2011). It can also support the formation of thin UTLS cirrus through anvil detrainment or by generating gravity waves where ice nucleates in the cold perturbations (Chang & L'Ecuyer, 2020; Jensen, Toon, Selkirk, et al., 1996; Jensen et al., 2016; Krämer et al., 2016).

Thin cirrus are common just below the cold point, especially around areas of frequent deep convection (Virts & Houze, 2015), with possible impacts on the UTLS from ice removal and radiative lofting (Fueglistaler et al., 2009; Jensen, Toon, Pfister, et al., 1996, Jensen, Toon, Selkirk, et al., 1996). An outstanding question is whether cold point-overshooting convection or thin cirrus has a greater impact on cold point temperatures and thus lower stratospheric moisture. Even global storm-resolving models, which explicitly simulate deep convection that reaches into the UTLS, have substantial intermodel spread in simulating the convection, cold point temperature, and cirrus that affect the UTLS (Nugent et al., 2022; Turbeville et al., 2022).

An important but imperfectly understood aspect of cold point-overshooting convection is its geographical and seasonal distribution, and how it differs between land and ocean regions. When defined using the 20 dBZ echo top height, the deepest tropical convection (Zipser et al., 2006) occurs mostly over land (e.g., N. Liu & Liu, 2016; N. Liu et al., 2020; Xian & Fu, 2015). But far too little large ice is typically lofted in cold point overshoots to reach such reflectivities. Other observational studies using more sensitive radar thresholds (e.g., −20 to −30 dBZ) to identify high convective cloud tops have found comparable frequencies of overshoots in convectively active land and ocean regions (Iwasaki et al., 2010; Li et al., 2022; Luo et al., 2008; Takahashi & Luo, 2014). Studies that used brightness temperature thresholds have even found more overshoots over oceans (Gettelman et al., 2002; Rossow & Pearl, 2007). The weaker land/ocean contrast in cold point overshoots versus in intense mid-tropospheric updrafts is not fully understood. The upper-tropospheric thermal environment surrounding very deep oceanic convection may be more conducive for relatively weaker updrafts to reach high altitudes (Kelley et al., 2010). Convective updraft velocity measurements in the UTLS are difficult and sparse, and extreme updraft strengths predicted by global storm-resolving models at 14 km altitude vary widely (Nugent et al., 2022).

A recent modeling study by Wu et al. (2023) found that in a warming climate, overshoots will increase much more over tropical oceans. Hong et al. (2005) and Aumann et al. (2018) also found warmer sea surface temperatures are correlated with more overshoots. Thus, documenting and understanding the spatial distribution of present-day cold point overshoots over ocean and land regions is important for predicting how overshooting convection may influence the UTLS in a changing climate.

Past studies using brightness temperature or −20 to −30 dBZ definitions of overshooting convection have been somewhat limited by relatively coarse data (Gettelman et al., 2002; Rossow & Pearl, 2007) or the twice-daily sun-synchronous sampling by the NASA A-Train (Li et al., 2022; Luo et al., 2008; Takahashi & Luo, 2014), which misses overshoots over land during the late afternoon diurnal cycle peak. Other studies used just 1 year of data (Iwasaki et al., 2010) or had only aggregate land-ocean statistics (Luo et al., 2008).

The goal of this paper is to achieve a climatology of the spatial distribution of cold point-overshooting convection across different land and ocean regions using a method that is generalizable to model output. Via calibration with active sensor data, we show more convincingly than prior studies that a combination of passive satellite brightness temperatures and reanalysis with frequent global coverage is now sufficiently accurate to develop the desired climatology. In 4 years of data, we find evidence of cold point-overshooting convection throughout the warmest, moistest parts of the tropics, with comparable frequencies over the Pacific warm pool and tropical land hot spots. Our proxy provides a useful observational benchmark for testing storm-resolving model simulations of tropical convective overshoot.

2. Data and Methods

2.1. Data Sets

We use ice water contents (IWC) from DARDAR-CLOUD v3.10 (Delanoë, 2023). The DARDAR product joins retrievals from the CloudSat cloud profiling radar and CALIPSO lidar on the NASA A-Train. The data have a horizontal footprint of 1.4 km and a vertical resolution of 60 m (Cazenave et al., 2019; Delanoë & Hogan, 2008, 2010). We use brightness temperatures from the NCEP/CPC L3 Half Hourly 4 km Global (60S–60N) Merged IR V1 (GPM_MERGIR) data set, which combines infrared brightness temperature data from several geostationary satellites (Janowiak et al., 2017). The GPM_MERGIR data set has a horizontal resolution of 4 km and a temporal resolution of 30 min.

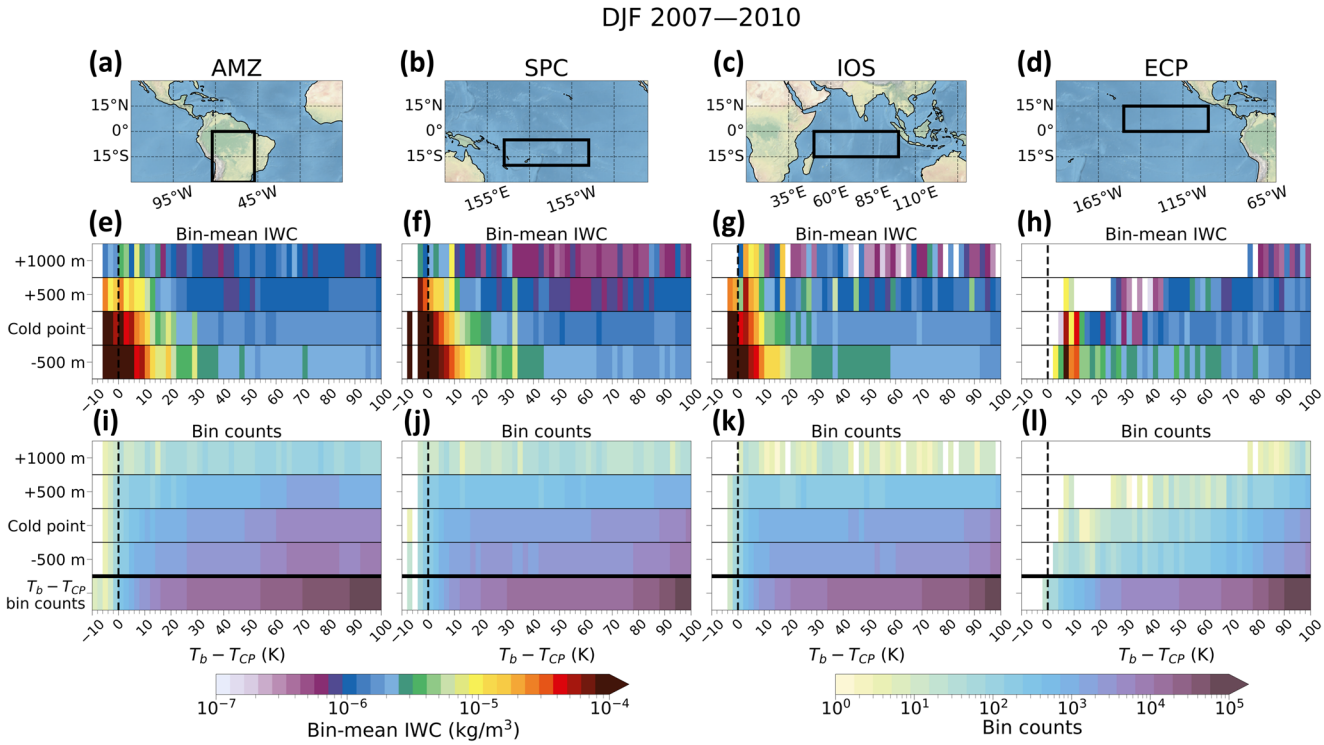

Figure 1. Cold point-relative cloud ice binned by $T_b - T_{CP}$ for all DARDAR pixels in DJF 2007–2010. (a–d) Maps of each analysis region; (e–h) bin-mean IWC at 500 m below to 1,000 m above the cold point height; and (i–l) bin counts conditioned on when DARDAR detects ice at each cold point-relative level. The row below the thick black line in (i–l) shows the total brightness temperature bin counts. The dashed lines in (e–l) mark where the brightness temperature equals the cold point. The bin width is 2 K.

Temperature profiles come from the ECMWF Reanalysis v5 (ERA5) model level data, which is available hourly on a 0.25° × 0.25° grid with a vertical resolution of 300–400 m in the UTLS (Hersbach et al., 2017). The ERA5 reanalysis incorporates both Global Navigation Satellite System Radio Occultation (GNSS-RO) data and radiosonde measurements into the upper-level temperatures (Hersbach et al., 2020). We use reanalysis rather than the GNSS-RO or radiosonde data directly to have a collocated cold point temperature for each DARDAR retrieval. Overshooting convection occurs so infrequently that further restricting to near-coincident DARDAR and GNSS-RO data would insufficiently sample overshoots.

We consider two seasons: December-January-February (DJF) and June-July-August (JJA). Our DARDAR climatology is limited to 2007–2010, after which CloudSat only operated during the daytime. The ERA5 and GPM_MERGIR data are mapped onto the DARDAR track by selecting the data point closest in space and time to each DARDAR retrieval. However, the mapped T_b values may not represent the true brightness temperatures at each pixel since the GPM_MERGIR and DARDAR data could be offset by up to 15 min.

2.2. Analysis Regions

We focus our analysis on four regions of approximately equal size for each season (Figures 1a–1d). These locations (three oceanic, one land) were selected to enclose areas of frequent active convection based on the climatological mean precipitation rate. For DJF, the regions are Amazonia (AMZ), the southern Indian Ocean (IOS), and the South Pacific Convergence Zone (SPC). For JJA, the analogous regions are Africa (AFR), the equatorial Indian Ocean (IOE), and the West Pacific (WPC). We also consider the East-Central Pacific (ECP) as a control, since this area rarely experiences deep convection as intense as that over the warmest oceans (e.g., C. Liu & Zipser, 2005; C. Liu et al., 2007), despite having similarly high time-mean precipitation rates. Table S1 in Supporting Information S1 lists the coordinates of each region. Across all regions, there are approximately 6.5M retrievals in DJF and 8.4M in JJA.

2.3. Cold Point Tropopause

We define the cold point as the level of the minimum temperature in the hourly 0.25° ERA5 temperature profiles. The 0.25° grid is small enough to capture fine spatiotemporal variations in the cold point but large enough to avoid interpreting individual convective cloud tops as cold point fluctuations. The 2007–2010 time-mean cold points (see Figure S1 in Supporting Information S1) are higher (>17 km) and colder (∼191 K) in DJF than in JJA (altitude <17 km and temperature ∼194 K), consistent with previous studies (e.g., Kim & Son, 2012; Seidel et al., 2001).

Compared to GNSS-RO and radiosonde data, the ERA5 climatological tropical cold point is generally <0.5 K warmer and ∼150 m lower (Tegtmeier et al., 2020), although local variations may be larger. Hoffmann and Spang (2022) calculated an uncertainty of ±120–200 m in the lapse rate tropopause (LRT) height globally for ERA5 reanalysis. The ERA5 cold point, typically at or 0.5–1 km above the LRT (Munchak & Pan, 2014; Pan et al., 2018; Tseng & Fu, 2017), likely has a comparable uncertainty. In Section 3.3 we identify cold point overshoots by binning CloudSat-detectable echoes at intervals of 500 m relative to the local ERA5 cold point height. Echoes in the bin 500 m above the cold point presumably will lie above the true cold point despite these uncertainties.

3. Cloud Ice Above the Cold Point

3.1. Stratospheric Cirrus and Brightness Temperatures

To focus on cirrus associated with convective cold point overshoots, we bin DARDAR cloud ice by the difference between the brightness temperature (T_b) and the collocated cold point temperature (T_{CP}). This method is similar to that of Dauhut and Hohenegger (2022), who identified very deep convection in GSRM output by binning ice by the outgoing longwave radiation (OLR). Since brightness temperatures vary much more than cold point temperatures, large values of $T_b - T_{CP}$ correspond to high T_b and vice versa. We vertically bin the DARDAR data at cold-point-relative altitude levels. The ERA5 cold point height has a standard deviation of about 600 m within each analysis region, so using fixed altitude levels could incorrectly identify cold point overshoots. Following Pan and Munchak (2011), we instead use levels −500, 0, +500, and +1,000 m relative to the local ERA5-estimated cold point height. We interpret "stratospheric" cirrus detected by DARDAR in the +500 and +1,000 m bins as very likely to lie above the cold point, despite uncertainties in measurement, reanalysis, and collocation.

Figure 1 shows the bin-mean IWC and bin counts at the cold point-relative levels in the four analysis regions shown in the top row. In all regions, cirrus is occasionally detected at least 500 m above the cold point across most of the $T_b - T_{CP}$ bins, corresponding to a broad range of brightness temperatures (bottom row). In fact, more stratospheric cirrus is collocated with high T_b than low T_b, which may seem counterintuitive. However, the coloring for overall count in each $T_b - T_{CP}$ bin (below the thick black line) indicates that there are many more bins with high than low brightness temperature. Thus, an atmospheric column with high T_b (i.e., relatively thin and/or low-lying cirrus) is much less likely to include cirrus above the cold point than one with low T_b.

When $T_b - T_{CP}$ is below ∼10 K, there is enhanced cloud ice (middle row; $\geq 5 \times 10^{-6}$ kg/m^3) at 500 m above the cold point in all regions except the ECP. At these low brightness temperatures, ice is almost always detected at 500 m above the cold point; that is, the stratospheric cirrus bin counts are almost the same as the total bin counts. Together, these bin means and counts suggest that some of the DARDAR-detected stratospheric cirrus may indicate overshooting tops in both land and warm ocean regions.

There is some seasonal variability in the bin means and counts (see Figure S2 in Supporting Information S1 for JJA), but the overall patterns between analogous regions in DJF and JJA are the same. One difference is that bin counts at the +500 m level are lower in the WPC (Figure S2f in Supporting Information S1) than in the SPC (Figure 1f), meaning cirrus above the cold point is rarer in JJA over the Pacific warm pool. The ECP (Figure S2h in Supporting Information S1) has more ice above the cold point in JJA than in DJF (Figure 1h), but still has much less than in other regions.

3.2. Identifying Cold Point-Overshooting Tops

Most of the detections of ice above the cold point in Figure 1 and Figure S2 in Supporting Information S1 are associated with thin cirrus clouds with high T_b. For the low $T_b - T_{CP}$ bins, the cirrus likely overlies deep

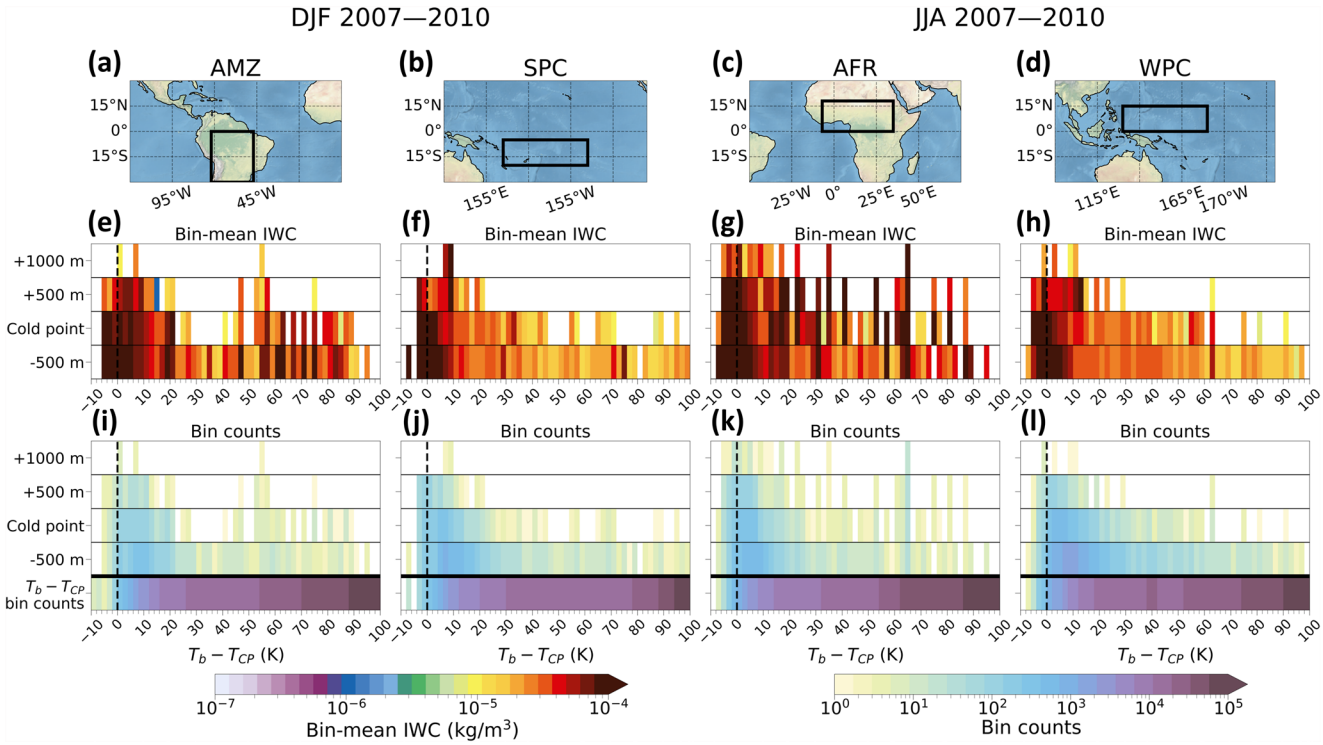

Figure 2. As in Figure 1 for select regions in DJF and JJA, but restricted to pixels in which the radar and lidar both detect ice.

convection. An actual overshooting top should not just have dense cloud ice but also larger ice particles lofted in the strong updraft that supports it; these particles should be detectable by the cloud radar. We therefore make binned plots restricted to include only radar-lidar pixels (Figure 2).

We anticipate that the dense cloud ice and low temperatures of overshooting tops should also cause particularly low brightness temperatures, possibly lower than the cold point temperature. The bottom row of Figure 2 shows that indeed, radar-detected ice above the cold point is almost exclusively associated with $T_b - T_{CP} < 10$ K, and at the coldest brightness temperatures, ice is almost always detected by the radar 500 m above the cold point. Thus we interpret radar/lidar-detected cirrus above the cold point as a cold point overshoot. We use the term "other stratospheric cirrus" for the remaining cirrus above the cold point that is detected only by lidar; some of this cirrus may be thin, while some of it may overlie extensive convective anvils or updrafts that do not overshoot the cold point.

Overshooting tops only comprise 1%–2% of all tropical stratospheric cirrus, as inferred by comparing the fraction of DARDAR cold point overshoot pixels containing ice at the +500 m level detected by both radar and lidar (Figure 2 and Figure S3 in Supporting Information S1) versus lidar-only detections. The occurrence frequency of other stratospheric cirrus (0.9%–2.5% in DJF, 0.4%–1.5% in JJA) is approximately 50–100 times larger than the convective overshoot occurrence frequency (0.01%–0.04% in both seasons). This relationship also holds for the ECP in JJA, but not in DJF when ice almost never occurs above the cold point there.

3.3. Brightness Temperature Proxy for Overshoots

Using the DARDAR data, we can infer a relationship between brightness temperature and cold point overshoots. If the relationship is strong enough, T_b, which is much more broadly available than radar/lidar data, can be confidently used as an overshoot proxy. The reliability of this proxy will depend on the infrared opacity of the cloud extending above the cold point. We expect cold point overshoots to be ice-rich, but whether their T_b over the size of a GPM_MERGIR pixel is necessarily less than the T_{CP} is less obvious.

We calibrate the brightness temperature proxy by finding the fraction of DARDAR detections at a given value of $T_b - T_{CP}$ that are associated with ice at 500 m above the cold point (top row in Figure 3). The probability of cold

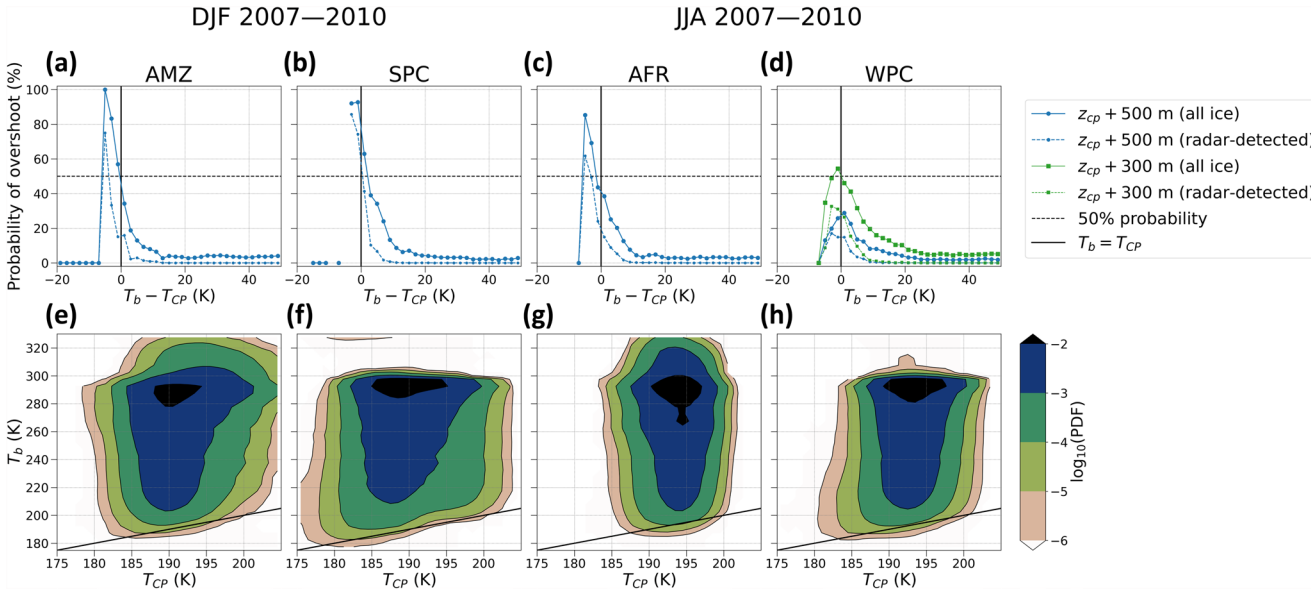

Figure 3. (a–d) Conditional probability of cold point overshoots (ice at 500 m above the cold point) as a function of $T_b - T_{CP}$ for all retrievals and radar-detected ice. The horizontal dashed line indicates a 50% chance of cold point overshoots. (e–h) Joint brightness temperature-cold point histograms for all GPM_MERGIR data points. In all panels, the solid lines mark where the brightness temperature equals the cold point. The same regions as in Figure 2 are shown.

point overshoots steadily increases once $T_b - T_{CP}$ falls below 10 K. In AFR, AMZ, and SPC, there is about a 50% chance of ice detected at 500 m above the cold point when $T_b = T_{CP}$ (solid lines in Figure 3). The probability of radar-detected ice (dashed lines in Figure 3) is slightly lower than for ice from all detections and does not exceed 50% when $T_b = T_{CP}$. The pattern is the same in the IOS and IOE (Figures S4a and S4c in Supporting Information S1). In the ECP, the probability of cold point overshoots never reaches 50%, and the brightness temperature is rarely less than the cold point (Figures S4b and S4d in Supporting Information S1). In the WPC, the probability of cold point overshoots at +500 m never exceeds 30%, but does exceed 50% at slightly lower heights (green lines in Figure 3h). Unlike in other regions, the conditional probability of a convective overshoot over the WPC does not monotonically increase as $T_b - T_{CP}$ becomes more negative; more investigation is needed to understand what other factors may enable $T_b < T_{CP}$ with a low conditional probability of stratospheric cirrus in this region. Luo et al. (2008) argued that $T_b < T_{CP}$ is an unreliable indicator of cold point overshoots because overshoots with (without) radar-detected ice above the cold point may have brightness temperatures warmer (colder) than the cold point. While this may be true for individual cases, our DARDAR results suggest that the $T_b < T_{CP}$ proxy is a statistically unbiased and physically plausible threshold for convective overshoots that are often CloudSat-detectable.

The joint histograms of brightness and cold point temperatures in the bottom row of Figure 3 show the probability distributions for the entire GPM_MERGIR data set (i.e., not conditioned on DARDAR retrievals) in each study region/season. These probability distributions are similar to those from Gettelman et al. (2002) for the global tropics. Despite the differently-shaped distributions between land and ocean, the percentage of data points where $T_b < T_{CP}$ (below the solid lines) is similar: 0.008/0.007% in AMZ/SPC and 0.024/0.015% in AFR/WPC. In both Indian Ocean regions, 0.004% of data points have $T_b < T_{CP}$, and there are even less in the ECP (0.0002% in DJF, 0.002% in JJA). These patterns suggest there are slightly more cold point overshoots over hot spots of tropical convection over land than over the warmest oceans, and that convective overshoots are rare over convectively active but slightly less warm ocean regions such as the Pacific Intertropical Convergence Zone.

Finally, in Figure 4 we apply this proxy to estimate the spatial distribution of cold point overshoots within our study regions over the entire 4-year GPM_MERGIR climatology, which past studies have not documented. With more data analysis, one could extend this analysis to look at the full global distribution and diurnal cycle of overshoots. Overshoots are 3–4 times more likely in JJA than DJF for analogous regions. Unsurprisingly, they are most common in AFR. Cold point overshoots are 30%–40% more frequent over land regions (AFR, AMZ) than the warmest ocean regions (WPC, SPC). On average, the regional frequencies of cold point overshoots for DJF are 0.011% in the AMZ, 0.008% in the SPC, 0.006% in the IOS, and negligible (0.0004%) in the ECP. In JJA,

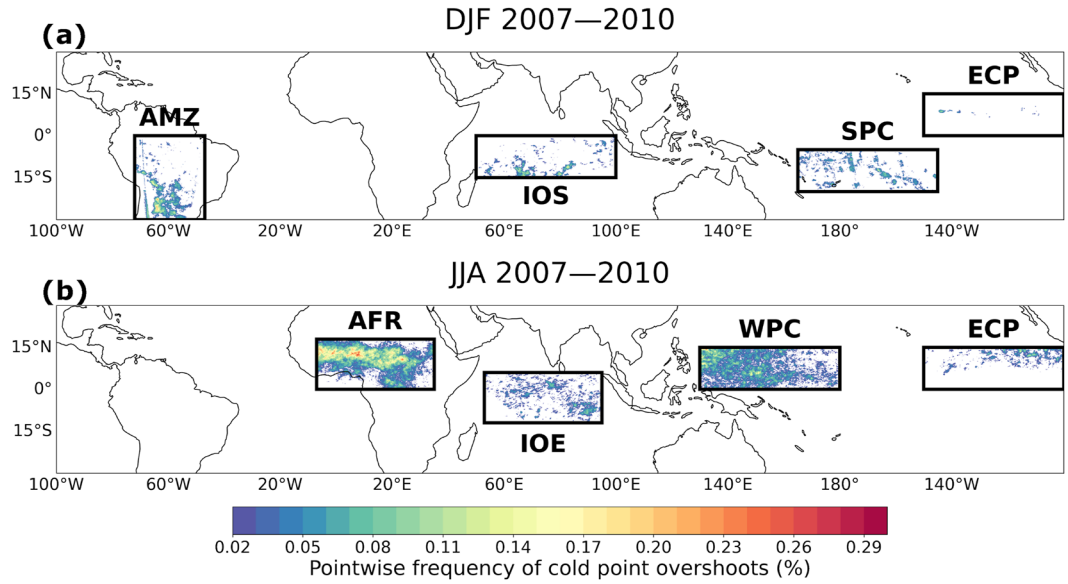

Figure 4. Frequency of cold point overshoots over time for (a) DJF and (b) JJA.

they are 0.045% in AFR, 0.032% in the WPC, 0.016% in the IOE, and 0.014% in the ECP. The frequencies of cold point overshoots and convective cirrus are similar everywhere but the SPC. Convective cirrus are much more frequent for the SPC, which may result from enhanced ascent from the Brewer-Dobson Circulation in the Pacific warm pool during boreal winter that can help maintain anvils produced by cold point-overshooting convection. Such anvils could be thick enough to be radar-detectable but not so thick that $T_b < T_{CP}$.

These results corroborate past findings that cold point overshoots somewhat favor tropical land areas over oceans from Luo et al. (2008) and other studies that defined convective overshoot using low radar reflectivity thresholds. Even if we adjust the proxy to $T_b - T_{CP} < -2$ K following the 50% probability of radar-detectable ice in Figure 3, this pattern is robust.

4. Conclusions

We argue that $T_b < T_{CP}$ is a suitable proxy to identify cold point overshoots that uses only high-resolution (4 km) IR brightness temperature from a geostationary satellite and ERA5-inferred cold point temperature. At such low brightness temperatures, we find that there is a high probability of cloud ice occurring above the cold point. Applying this proxy to 4 years of data over convectively active tropical land and ocean regions, we corroborate past findings that cold point-overshooting convection is only about 30%–40% more common over land (AFR and AMZ) than Pacific warm pool regions (WPC and SPC). The cooler East Pacific region (ECP) has very few cold point overshoots, and the Indian Ocean regions (IOE and IOS) fall somewhere in between. Even in the regions where cold point overshoots are the most frequent, thin cirrus above the cold point cover ∼100 times more area than the cold point-overshooting tops. By using more data than available to earlier investigators, we obtain seasonal maps of the overshoot frequency over our study regions that sample the full diurnal cycle and could easily be extended to the global tropics.

Our finding that cold point overshoots are comparably frequent between warm land and ocean areas does not contradict the widely-held view that convection is more intense over land. Oceanic convection has been well-documented to contain weaker and narrower updrafts (e.g., Fierro et al., 2012; LeMone & Zipser, 1980; Zipser & LeMone, 1980). Other classic measures of convective intensity where land dominates, including frequent lightning and tall 40 dBZ echo top heights (Zipser et al., 2006), need not always coincide with overshooting tops above the cold point. We expect that the cold point overshoots we have identified over land are more intense by these measures than those we have identified over oceans, but this does not necessarily imply less frequent cold point overshoots.

In a follow-up paper, we will adapt our $T_b < T_{CP}$ proxy to global storm-resolving model (GSRM) output from the DYAMOND intercomparison (Stevens et al., 2019) to compare cold point overshoots between models and

observations. GSRMs explicitly simulate deep convection and have small enough horizontal grid spacing to capture convective overshoots. Understanding how well GSRMs can reproduce observed cold point overshoots in the current climate over both land and ocean will test the reliability of these models for simulating cold point overshoots and their influence on the UTLS in a warming climate.

Data Availability Statement

DARDAR data was provided by NASA and is available from the AERIS/ICARE Data and Services Center in Delanoë (2023). ERA5 reanalysis is available in Hersbach et al. (2017) and was downloaded using the CDS API from the Copernicus Climate Change Service. NCEP/CPC GPM_MERGIR data is available from NASA GES DISC in Janowiak et al. (2017). All code used for this analysis is available on GitHub and stored in Nugent (2023).

Acknowledgments
JN was supported by the National Science Foundation through the Partnerships in International Research and Education program under Grant OISE-1743753. CB was supported by the Allen Institute for AI. Data management was provided by the German Climate Computing Center (DKRZ) and supported through the projects ESiWACE and ESiWACE2, which have received funding from the European Union's Horizon 2020 research and innovation program under grant agreements No 675191 and 823988. This work used resources of the DKRZ granted by its Scientific Steering Committee (WLA) under project IDs bk1040 and bb1153.

References

Aumann, H. H., Behrangi, A., & Wang, Y. (2018). Increased frequency of extreme tropical deep convection: AIRS observations and climate model predictions. *Geophysical Research Letters*, *45*(24), 13530–13537. https://doi.org/10.1029/2018GL079423

Brewer, A. W. (1949). Evidence for a world circulation provided by the measurements of helium and water vapour distribution in the stratosphere. *Quarterly Journal of the Royal Meteorological Society*, *75*(326), 351–363. https://doi.org/10.1002/qj.49707532603

Bucci, S., Legras, B., Sellitto, P., D'Amato, F., Viciani, S., Montori, A., et al. (2020). Deep-convective influence on the upper troposphere–lower stratosphere composition in the Asian monsoon anticyclone region: 2017 StratoClim campaign results. *Atmospheric Chemistry and Physics*, *20*(20), 12193–12210. https://doi.org/10.5194/acp-20-12193-2020

Cazenave, Q., Ceccaldi, M., Delanoë, J., Pelon, J., Groß, S., & Heymsfield, A. (2019). Evolution of DARDAR-CLOUD ice cloud retrievals: New parameters and impacts on the retrieved microphysical properties. *Atmospheric Measurement Techniques*, *12*(5), 2819–2835. https://doi.org/10.5194/amt-12-2819-2019

Chae, J. H., Wu, D. L., Read, W. G., & Sherwood, S. C. (2011). The role of tropical deep convective clouds on temperature, water vapor, and dehydration in the tropical tropopause layer (TTL). *Atmospheric Chemistry and Physics*, *11*(8), 3811–3821. https://doi.org/10.5194/acp-11-3811-2011

Chang, K.-W., & L'Ecuyer, T. (2020). Influence of gravity wave temperature anomalies and their vertical gradients on cirrus clouds in the tropical tropopause layer—A satellite-based view. *Atmospheric Chemistry and Physics*, *20*(21), 12499–12514. https://doi.org/10.5194/acp-20-12499-2020

Corti, T., Luo, B. P., de Reus, M., Brunner, D., Cairo, F., Mahoney, M. J., et al. (2008). Unprecedented evidence for deep convection hydrating the tropical stratosphere: Convective hydration. *Geophysical Research Letters*, *35*(10), L10810. https://doi.org/10.1029/2008GL033641

Dauhut, T., & Hohenegger, C. (2022). The contribution of convection to the stratospheric water vapor: The first budget using a global storm-resolving model. *Journal of Geophysical Research: Atmospheres*, *127*(5), e2021JD036295. https://doi.org/10.1029/2021JD036295

Delanoë, J. (2023). DARDAR cloud—Heymfield's composite mass-size relationship. DARDAR-CLOUD v3.10 [Dataset]. Aeris. https://doi.org/10.25326/449

Delanoë, J., & Hogan, R. J. (2008). A variational scheme for retrieving ice cloud properties from combined radar, lidar, and infrared radiometer. *Journal of Geophysical Research*, *113*(D7), D07204. https://doi.org/10.1029/2007JD009000

Delanoë, J., & Hogan, R. J. (2010). Combined CloudSat-CALIPSO-MODIS retrievals of the properties of ice clouds. *Journal of Geophysical Research*, *115*, D00H29. https://doi.org/10.1029/2009JD012346

Dessler, A. E. (2002). The effect of deep, tropical convection on the tropical tropopause layer. *Journal of Geophysical Research*, *107*(D3), 4033. https://doi.org/10.1029/2001JD000511

Dessler, A. E., Ye, H., Wang, T., Schoeberl, M., Oman, L., Douglass, A., et al. (2016). Transport of ice into the stratosphere and the humidification of the stratosphere over the 21st century. *Geophysical Research Letters*, *43*(5), 2323–2329. https://doi.org/10.1002/2016GL067991

Dion, I.-A., Ricaud, P., Haynes, P., Carminati, F., & Dauhut, T. (2019). Ice injected into the tropopause by deep convection—Part 1: In the austral convective tropics. *Atmospheric Chemistry and Physics*, *19*(9), 6459–6479. https://doi.org/10.5194/acp-19-6459-2019

Fierro, A. O., Zipser, E. J., LeMone, M. A., Straka, J. M., & Simpson, J. M. (2012). Tropical oceanic hot towers: Need they be undilute to transport energy from the boundary layer to the upper troposphere effectively? An answer based on trajectory analysis of a simulation of a TOGA COARE convective system. *Journal of the Atmospheric Sciences*, *69*(1), 195–213. https://doi.org/10.1175/JAS-D-11-0147.1

Fueglistaler, S., Dessler, A. E., Dunkerton, T. J., Folkins, I., Fu, Q., & Mote, P. W. (2009). Tropical tropopause layer. *Reviews of Geophysics*, *47*(1). https://doi.org/10.1029/2008RG000267

Gettelman, A., Salby, M. L., & Sassi, F. (2002). Distribution and influence of convection in the tropical tropopause region: Convection in the tropopause region. *Journal of Geophysical Research*, *107*(D10), ACL6-1–ACL6-12. https://doi.org/10.1029/2001JD001048

Hersbach, H., Bell, B., Berrisford, P., Hirahara, S., Horányi, A., Muñoz-Sabater, J., et al. (2020). The ERA5 global reanalysis. *Quarterly Journal of the Royal Meteorological Society*, *146*(730), 1999–2049. https://doi.org/10.1002/qj.3803

Hersbach, H., Bell, B., Berrisford, P., Hirahara, S., Horányi, A., Muñoz-Sabater, J., et al. (2017). Complete ERA5 from 1940: Fifth generation of ECMWF atmospheric reanalyses of the global climate. [Dataset]. Copernicus Climate Change Service (C3S) Data Store (CDS). https://doi.org/10.24381/cds.143582cf

Hoffmann, L., & Spang, R. (2022). An assessment of tropopause characteristics of the ERA5 and ERA-Interim meteorological reanalyses. *Atmospheric Chemistry and Physics*, *22*(6), 4019–4046. https://doi.org/10.5194/acp-22-4019-2022

Holton, J. R., & Gettelman, A. (2001). Horizontal transport and the dehydration of the stratosphere. *Geophysical Research Letters*, *28*(14), 2799–2802. https://doi.org/10.1029/2001GL013148

Hong, G., Heygster, G., Miao, J., & Kunzi, K. (2005). Detection of tropical deep convective clouds from AMSU-B water vapor channels measurements. *Journal of Geophysical Research*, *110*(D5), D05205. https://doi.org/10.1029/2004JD004949

Iwasaki, S., Shibata, T., Nakamoto, J., Okamoto, H., Ishimoto, H., & Kubota, H. (2010). Characteristics of deep convection measured by using the A-train constellation. *Journal of Geophysical Research*, *115*(D6), D06207. https://doi.org/10.1029/2009JD013000

Janowiak, J., Joyce, B., & Xie, P. (2017). NCEP/CPC L3 half hourly 4km global (60S–60N) merged IR V1 [Dataset]. In A. Savtchenko, & M. D. Greenbelt (Eds.) *Goddard Earth sciences data and information Services center (GES DISC)*. https://doi.org/10.5067/P4HZB9N27EKU

Jensen, E. J., Ackerman, A. S., & Smith, J. A. (2007). Can overshooting convection dehydrate the tropical tropopause layer? *Journal of Geophysical Research*, *112*(D11), D11209. https://doi.org/10.1029/2006JD007943

Jensen, E. J., Toon, O. B., Pfister, L., & Selkirk, H. B. (1996). Dehydration of the upper troposphere and lower stratosphere by subvisible cirrus clouds near the tropical tropopause. *Geophysical Research Letters*, *23*(8), 825–828. https://doi.org/10.1029/96GL00722

Jensen, E. J., Ueyama, R., Pfister, L., Bui, T. V., Alexander, M. J., Podglajen, A., et al. (2016). High-frequency gravity waves and homogeneous ice nucleation in tropical tropopause layer cirrus: Waves and ice nucleation. *Geophysical Research Letters*, *43*(12), 6629–6635. https://doi.org/10.1002/2016GL069426

Jensen, E. J., Toon, O. B., Selkirk, H. B., Spinhirne, J. D., & Schoeberl, M. R. (1996). On the formation and persistence of subvisible cirrus clouds near the tropical tropopause. *Journal of Geophysical Research*, *101*(D16), 21361–21375. https://doi.org/10.1029/95JD03575

Kelley, O. A., Stout, J., Summers, M., & Zipser, E. J. (2010). Do the tallest convective cells over the tropical ocean have slow updrafts? *Monthly Weather Review*, *138*(5), 1651–1672. https://doi.org/10.1175/2009MWR3030.1

Khaykin, S. M., Moyer, E., Krämer, M., Clouser, B., Bucci, S., Legras, B., et al. (2022). Persistence of moist plumes from overshooting convection in the Asian monsoon anticyclone. *Atmospheric Chemistry and Physics*, *22*(5), 3169–3189. https://doi.org/10.5194/acp-22-3169-2022

Kim, J., & Son, S.-W. (2012). Tropical cold-point tropopause: Climatology, seasonal cycle, and intraseasonal variability derived from COSMIC GPS radio occultation measurements. *Journal of Climate*, *25*(15), 5343–5360. https://doi.org/10.1175/JCLI-D-11-00554.1

Krämer, M., Rolf, C., Luebke, A., Afchine, A., Spelten, N., Costa, A., et al. (2016). A microphysics guide to cirrus clouds—Part 1: Cirrus types. *Atmospheric Chemistry and Physics*, *16*(5), 3463–3483. https://doi.org/10.5194/acp-16-3463-2016

Kuang, Z., & Bretherton, C. S. (2004). Convective influence on the heat balance of the tropical tropopause layer: A cloud-resolving model study. *Journal of the Atmospheric Sciences*, *61*(23), 2919–2927. https://doi.org/10.1175/JAS-3306.1

LeMone, M. A., & Zipser, E. J. (1980). Cumulonimbus vertical velocity events in GATE. Part I: Diameter, intensity and mass flux. *Journal of the Atmospheric Sciences*, *37*(11), 2444–2457. https://doi.org/10.1175/1520-0469(1980)037⟨2444:CVVEIG⟩2.0.CO;2

Li, H., Wei, X., Min, M., Li, B., Nong, Z., & Chen, L. (2022). A dataset of overshooting cloud top from 12-year CloudSat/CALIOP joint observations. *Remote Sensing*, *14*(10), 2417. https://doi.org/10.3390/rs14102417

Liu, C., & Zipser, E. J. (2005). Global distribution of convection penetrating the tropical tropopause. *Journal of Geophysical Research*, *110*(D23), D23104. https://doi.org/10.1029/2005JD006063

Liu, C., Zipser, E. J., & Nesbitt, S. W. (2007). Global distribution of tropical deep convection: Different perspectives from TRMM infrared and radar data. *Journal of Climate*, *20*(3), 489–503. https://doi.org/10.1175/JCLI4023.1

Liu, N., & Liu, C. (2016). Global distribution of deep convection reaching tropopause in 1 year GPM observations. *Journal of Geophysical Research: Atmospheres*, *121*(8), 3824–3842. https://doi.org/10.1002/2015JD024430

Liu, N., Liu, C., & Hayden, L. (2020). Climatology and detection of overshooting convection from 4 years of GPM precipitation radar and passive microwave observations. *Journal of Geophysical Research: Atmospheres*, *125*(7), e2019JD032003. https://doi.org/10.1029/2019JD032003

Luo, Z., Liu, G. Y., & Stephens, G. L. (2008). CloudSat adding new insight into tropical penetrating convection. *Geophysical Research Letters*, *35*(19), L19819. https://doi.org/10.1029/2008GL035330

Munchak, L. A., & Pan, L. L. (2014). Separation of the lapse rate and the cold point tropopauses in the tropics and the resulting impact on cloud top-tropopause relationships. *Journal of Geophysical Research: Atmospheres*, *119*(13), 7963–7978. https://doi.org/10.1002/2013JD021189

Nugent, J. M. (2023). jacnugent/tropical-conv-os-2023: Published version of the software (Version v1.0.0) [Software]. Zenodo. https://doi.org/10.5281/ZENODO.8430593

Nugent, J. M., Turbeville, S. M., Bretherton, C. S., Blossey, P. N., & Ackerman, T. P. (2022). Tropical cirrus in global storm-resolving models: 1. Role of deep convection. *Earth and Space Science*, *9*(2). https://doi.org/10.1029/2021EA001965

Pan, L. L., Honomichl, S. B., Bui, T. V., Thornberry, T., Rollins, A., Hintsa, E., & Jensen, E. J. (2018). Lapse rate or cold point: The tropical tropopause identified by in situ trace gas measurements. *Geophysical Research Letters*, *45*(19), 10756–10763. https://doi.org/10.1029/2018GL079573

Pan, L. L., & Munchak, L. A. (2011). Relationship of cloud top to the tropopause and jet structure from CALIPSO data. *Journal of Geophysical Research*, *116*(D12), D12201. https://doi.org/10.1029/2010JD015462

Pommereau, J.-P. (2010). Troposphere-to-stratosphere transport in the tropics. *Comptes Rendus Geoscience*, *342*(4–5), 331–338. https://doi.org/10.1016/j.crte.2009.10.015

Randel, W. J., & Jensen, E. J. (2013). Physical processes in the tropical tropopause layer and their roles in a changing climate. *Nature Geoscience*, *6*(3), 169–176. https://doi.org/10.1038/ngeo1733

Randel, W. J., & Park, M. (2019). Diagnosing observed stratospheric water vapor relationships to the cold point tropical tropopause. *Journal of Geophysical Research: Atmospheres*, *124*(13), 7018–7033. https://doi.org/10.1029/2019JD030648

Randel, W. J., Wu, F., Oltmans, S. J., Rosenlof, K., & Nedoluha, G. E. (2004). Interannual changes of stratospheric water vapor and correlations with tropical tropopause temperatures. *Journal of the Atmospheric Sciences*, *61*(17), 2133–2148. https://doi.org/10.1175/1520-0469(2004)061⟨2133:ICOSWV⟩2.0.CO;2

Rossow, W. B., & Pearl, C. (2007). 22-Year survey of tropical convection penetrating into the lower stratosphere. *Geophysical Research Letters*, *34*(4), L04803. https://doi.org/10.1029/2006GL028635

Seidel, D. J., Ross, R. J., Angell, J. K., & Reid, G. C. (2001). Climatological characteristics of the tropical tropopause as revealed by radiosondes. *Journal of Geophysical Research*, *106*(D8), 7857–7878. https://doi.org/10.1029/2000JD900837

Solomon, S., Rosenlof, K. H., Portmann, R. W., Daniel, J. S., Davis, S. M., Sanford, T. J., & Plattner, G.-K. (2010). Contributions of stratospheric water vapor to decadal changes in the rate of global warming. *Science*, *327*(5970), 1219–1223. https://doi.org/10.1126/science.1182488

Stevens, B., Satoh, M., Auger, L., Biercamp, J., Bretherton, C. S., Chen, X., et al. (2019). DYAMOND: The DYnamics of the atmospheric general circulation modeled on non-hydrostatic domains. *Progress in Earth and Planetary Science*, *6*(1), 61. https://doi.org/10.1186/s40645-019-0304-z

Takahashi, H., & Luo, Z. J. (2014). Characterizing tropical overshooting deep convection from joint analysis of CloudSat and geostationary satellite observations: Tropical deep convection by CloudSat. *Journal of Geophysical Research: Atmospheres*, *119*(1), 112–121. https://doi.org/10.1002/2013JD020972

Tegtmeier, S., Anstey, J., Davis, S., Dragani, R., Harada, Y., Ivanciu, I., et al. (2020). Temperature and tropopause characteristics from reanalyses data in the tropical tropopause layer. *Atmospheric Chemistry and Physics*, *20*(2), 753–770. https://doi.org/10.5194/acp-20-753-2020

Tian, W., Huang, J., Zhang, J., Xie, F., Wang, W., & Peng, Y. (2023). Role of stratospheric processes in climate change: Advances and challenges. *Advances in Atmospheric Sciences*, *40*(8), 1379–1400. https://doi.org/10.1007/s00376-023-2341-1

Tseng, H.-H., & Fu, Q. (2017). Tropical tropopause layer cirrus and its relation to tropopause. *Journal of Quantitative Spectroscopy and Radiative Transfer*, *188*, 118–131. https://doi.org/10.1016/j.jqsrt.2016.05.029

Turbeville, S. M., Nugent, J. M., Ackerman, T. P., Bretherton, C. S., & Blossey, P. N. (2022). Tropical cirrus in global storm-resolving models: 2. Cirrus life cycle and top-of-atmosphere radiative fluxes. *Earth and Space Science*, *9*(2). https://doi.org/10.1029/2021EA001978

Ueyama, R., Schoeberl, M., Jensen, E., Pfister, L., Park, M., & Ryoo, J.-M. (2023). Convective impact on the global lower stratospheric water vapor budget. *Journal of Geophysical Research: Atmospheres*, *128*(6), e2022JD037135. https://doi.org/10.1029/2022JD037135

Vernier, J.-P., Pommereau, J.-P., Thomason, L. W., Pelon, J., Garnier, A., Deshler, T., et al. (2011). Overshooting of clean tropospheric air in the tropical lower stratosphere as seen by the CALIPSO lidar. *Atmospheric Chemistry and Physics*, *11*(18), 9683–9696. https://doi.org/10.5194/acp-11-9683-2011

Virts, K. S., & Houze, R. A. (2015). Clouds and water vapor in the tropical tropopause transition layer over mesoscale convective systems. *Journal of the Atmospheric Sciences*, *72*(12), 4739–4753. https://doi.org/10.1175/JAS-D-15-0122.1

Wu, X., Fu, Q., & Kodama, C. (2023). Response of tropical overshooting deep convection to global warming based on global cloud-resolving model simulations. *Geophysical Research Letters*, *50*(14), e2023GL104210. https://doi.org/10.1029/2023GL104210

Xian, T., & Fu, Y. (2015). Characteristics of tropopause-penetrating convection determined by TRMM and COSMIC GPS radio occultation measurements. *Journal of Geophysical Research: Atmospheres*, *120*(14), 7006–7024. https://doi.org/10.1002/2014JD022633

Zhou, X. L., Geller, M. A., & Zhang, M. H. (2001). Tropical cold point tropopause characteristics derived from ECMWF reanalyses and soundings. *Journal of Climate*, *14*(8), 1823–1838. https://doi.org/10.1175/1520-0442(2001)014⟨1823:TCPTCD⟩2.0.CO;2

Zipser, E. J., Cecil, D. J., Liu, C., Nesbitt, S. W., & Yorty, D. P. (2006). Where are the most intense thunderstorms on Earth? *Bulletin of the American Meteorological Society*, *87*(8), 1057–1072. https://doi.org/10.1175/BAMS-87-8-1057

Zipser, E. J., & LeMone, M. A. (1980). Cumulonimbus vertical velocity events in GATE. Part II: Synthesis and model core structure. *Journal of the Atmospheric Sciences*, *37*(11), 2458–2469. https://doi.org/10.1175/1520-0469(1980)037⟨2458:CVVEIG⟩2.0.CO;2